Acta Crystallographica Section D
**Biological Crystallography**
ISSN 0907-4449

# The high-resolution structure of pig heart succinyl-CoA:3-oxoacid coenzyme A transferase

**Shu-Fen Coker,[a] Adrian J. Lloyd,[b]‡ Edward Mitchell,[c] Gareth R. Lewis,[b] Alun R. Coker[a]* and Peter M. Shoolingin-Jordan[b]**

[a]Center for Amyloidosis and Acute Phase Proteins, Division of Medicine (Royal Free Campus), University College London, Rowland Hill Street, London NW3 2PF, England, [b]School of Biological Sciences, University of Southampton, Southampton, Hampshire SO16 7PX, England, and [c]ESRF, 6 Rue Jules Horowitz, BP 220, 38043 Grenoble CEDEX 9, France

‡ Present address: Department of Biological Sciences, Gibbet Hill Road, University of Warwick, Coventry CV4 7AL, England.

Correspondence e-mail: a.coker@medsch.ucl.ac.uk

Received 5 March 2010
Accepted 17 May 2010

**PDB Reference:** succinyl-CoA:3-oxoacid-coenzyme A transferase, 3k6m.

The enzyme succinyl-CoA:3-oxoacid coenzyme A transferase (SCOT) participates in the metabolism of ketone bodies in extrahepatic tissues. It catalyses the transfer of coenzyme A (CoA) from succinyl-CoA to acetoacetate with a classical ping-pong mechanism. There is biochemical evidence that the enzyme undergoes conformational changes during the reaction, but no domain movements have been reported in the available crystal structures. Here, a structure of pig heart SCOT refined at 1.5 Å resolution is presented, showing that one of the four enzyme subunits in the crystallographic asymmetric unit has a molecule of glycerol bound in the active site; the glycerol molecule is hydrogen bonded to the conserved catalytic glutamate residue and is likely to occupy the cosubstrate-binding site. The binding of glycerol is associated with a substantial relative movement (a 13° rotation) of two previously undefined domains that close around the substrate-binding site. The binding orientation of one of the cosubstrates, acetoacetate, is suggested based on the glycerol binding and the possibility that this dynamic domain movement is of functional importance is discussed.

## 1. Introduction

Ketone bodies (acetoacetate, 3-hydroxybutyrate and acetone) are generated by hepatic fatty-acid catabolism and are transported in the blood to the extrahepatic tissues, where acetoacetate and 3-hydroxybutyrate are used as an energy source. For use as an energy source, 3-hydroxybutyrate is first converted to acetoacetate by *R*-3-hydroxybutyrate dehydrogenase (EC 1.1.1.30). Acetoacetate, which is produced either from 3-hydroxybutyrate or directly from ketogenesis, is activated by the transfer of CoA from succinyl-CoA in a reaction catalysed by succinyl-CoA:3-oxoacid CoA transferase (SCOT; EC 2.8.3.5). Acetoacetyl-CoA is then cleaved by thiolase (EC 2.3.1.9), yielding two molecules of acetyl-CoA which enter the citric acid cycle. A few cases of individuals with SCOT deficiency have been reported (Song *et al.*, 1998; Fukao *et al.*, 2000, 2007). Owing to the build-up of unused ketone bodies in the blood, these unfortunate individuals suffer chronic ketosis and lapse into ketoacidosis during episodes of disease or starvation.

CoA transferases can be grouped into three families (Heider, 2001) defined by their mechanism and structure. SCOT belongs to family I, the evolutionarily conserved members of which share a common ping-pong mechanism and are usually heterotetramers or heterooctamers ($\alpha_2\beta_2$ or $\alpha_4\beta_4$). Mammalian SCOT and *Escherichia coli* YdiF are exceptions, consisting of homodimers or homotetramers of a single polypeptide that contains two subdomains orthologous to the

$\alpha$ and $\beta$ subunits of the other members of family I. Both subunits share a common $\alpha/\beta/\alpha$ architecture with a central seven-stranded $\beta$-sheet and belong to the NagB/RipA/CoA transferase superfamily. In the Structural Classification of Proteins database (SCOP; Murzin *et al.*, 1995) the $\alpha$ and $\beta$ subunits define the 'CoA transferase $\alpha$-like' and 'CoA transferase $\beta$-like' fold families, respectively. Crystal structures are available for several family I CoA transferases, including glutaconate CoA transferase (GCT) from *Acidaminococcus fementens* (Jacob *et al.*, 1997), the $\alpha$ subunit of *E. coli* acetate CoA transferase (Korolev *et al.*, 2002), YdiF from *E. coli* (Rangarajan *et al.*, 2005), *Sus scrofa* (pig) SCOT (Bateman *et al.*, 2002; PDB code 1o9l, E. P. Mitchell, A. J. Lloyd, G. Lewis & P. Shoolingin-Jordan, unpublished work; Coros *et al.*, 2004; Tammam *et al.*, 2007) and human SCOT (PDB code 3dlx; K. L. Kavanagh, N. Shafqat, W. W. Yue, S. Picaud, J. W. Murray, E. M. Maclean, F. von Delft, A. K. Roos, C. H. Arrowsmith, M. Wikstrom, A. M. Edwards, C. Bountra & U. Oppermann, unpublished work). All of these structures share the same fold, with a single subunit of SCOT and YdiF corresponding to a heterodimer of GCT. The $\alpha$ subunit of GCT corresponds to the amino-terminal residues of SCOT and YdiF, whilst the $\beta$ subunit of GCT corresponds to the C-terminal domain. The amino-terminal and C-terminal structural domains of SCOT and YdiF are linked by a protease-sensitive linker peptide termed the 'hinge' region. This linker peptide is not visible in the SCOT and YdiF structures, suggesting that it is highly flexible. Owing to their common fold, the $\alpha$ and $\beta$ domains of GCT and the N- and C-terminal domains of YdiF have been to proposed to be the product of an ancient gene-duplication event (Jacob *et al.*, 1997; Rangarajan *et al.*, 2005).

SCOT transfers CoA from succinyl-CoA to acetoacetate with a classical ping-pong mechanism (Hersh & Jencks, 1967). Central to this mechanism is a glutamate residue of the enzyme (Glu305 in most mammalian enzymes) which attacks the carbonyl C atom of the thioester of the incoming succinyl-CoA substrate, leading to the generation of a succinyl–Glu305 mixed anhydride (Solomon & Jencks, 1969; Rochet & Bridger, 1994; Pickart & Jencks, 1979). The glutamyl carbonyl C atom of this anhydride is then subject to nucleophilic attack by the thiol of CoA to generate a SCOT–CoA thioester, which is the first isolatable intermediate. Acetoacetate, the recipient of the CoA, then attacks the glutamyl carbonyl C atom of the SCOT–CoA thioester, generating a second anhydride. Finally, the CoA attacks the acetoacetyl–Glu305 mixed anhydride on the acetoacetyl carbonyl C atom to form acetoacetyl-CoA and free enzyme.

It has been proposed that the formation of the SCOT–CoA intermediate involves significant conformational change. The reaction of the dimeric SCOT–CoA intermediate with either succinate or acetoacetate results in only one half of the CoA being transferred to the acceptor, suggesting a conformational change mediating half-of-the-sites reactivity (Lloyd & Shoolingin-Jordan, 2001). A database analysis of a group of non-redundant enzymes for which apo and ligand-bound structures were available in the PDB has also shown that transferases often undergo large rigid-body domain motions, closing a cleft to bury reactive intermediates inside the molecule and protecting them from reaction with the bulk solvent (Koike *et al.*, 2008). Although no structures of SCOT–CoA intermediates are available, a structural comparison of apo SCOT with the CoA-bound complex of YdiF, a structurally homologous enzyme from *E. coli*, shows that significant domain movements must occur in order for apo SCOT to bind CoA. Based on superimposing the N- and C-terminal domains of apo SCOT onto the equivalent domains of the YdiF–CoA intermediate, a model has been proposed which predicts that the N- and C-terminal domains of SCOT would close by a 17° rotation on binding CoA (Tammam *et al.*, 2007).

Here, we present the crystal structure of dimeric pig heart SCOT which, although crystallized without natural substrates, reveals new dynamic domains in one of the four subunits in the asymmetric unit. Unlike the dynamic domain movements based on the N- and C-terminal domains, the new dynamic domain movement would not disrupt the dimer interface and provides a credible model for the domain movements proposed during the catalytic cycle. This subunit also contains clear electron density for a glycerol molecule in the active site, which we believe binds in an analogous way to the cosubstrate acetoacetate.

## 2. Materials and methods

### 2.1. Protein purification, crystallization and X-ray data collection

SCOT was purified from porcine heart as described previously (Lloyd & Shoolingin-Jordan, 2001) and was stored at 10–15 mg ml$^{-1}$ in 20 m*M* 3-(*N*-morpholino)propanesulfonic acid (MOPS) pH 7.2 containing 1 m*M* EDTA, 1 m*M* DTT, 0.2 m*M* PMSF and 10%(*v*/*v*) glycerol. Crystals of the enzyme were grown using the hanging-drop method at 277 K. An 8 µl drop consisting of 4 µl enzyme stock and 4 µl precipitant was suspended over a 1 ml reservoir containing precipitant [75 m*M* Tris–HCl pH 8.0, 18–22%(*w*/*v*) PEG 3350 or PEG 4000]. The best-quality crystals were obtained after 24–48 h in 20% PEG. The single crystal used for the diffraction experiment was soaked for 1 h in a cryoprotectant based on the precipitant solution supplemented with 25%(*v*/*v*) glycerol before being vitrified in a cold nitrogen stream at 100 K. Diffraction data were collected on beamline ID14-3 at the ESRF (Grenoble, France) with the wavelength set to 0.948 Å using a MAR CCD (133 mm) detector. Data to a resolution of 1.5 Å were indexed, integrated and scaled using the *CCP*4 programs *MOSFLM*, *SCALA* and *TRUNCATE* (Collaborative Computational Project, Number 4,1994). Data-collection statistics are presented in Table 1.

### 2.2. Structure determination and analysis

Phases were determined by the molecular-replacement method using the program *AMoRe* (Navaza, 1994). Subunit *A* from our previously determined SCOT structure (PDB code 1o9l) stripped of waters was used as the search probe. The SCOT model consisting of four subunits was refined using

**Table 1**
Crystallographic statistics.

Values in parentheses are for the highest resolution shell.

| | |
|---|---|
| Space group | $P2_1$ |
| Unit-cell parameters | |
| $a$ (Å) | 73.72 |
| $b$ (Å) | 133.57 |
| $c$ (Å) | 102.23 |
| $\beta$ (°) | 104.98 |
| Resolution (Å) | 20.1–1.50 (1.54–1.50) |
| No. of measurements | 993659 (40939) |
| No. of unique reflections | 297163 (18372) |
| Redundancy | 3.3 (2.2) |
| $R_{\rm p.i.m.}$† (%) | 3.9 (24.8) |
| $I/\sigma(I)$ | 12.0 (2.3) |
| Completeness (%) | 97.7 (82.1) |
| Wilson $B$ factor (Å$^2$) | 17.2 |
| $R_{\rm work}$‡ (%) | 16.5 |
| $R_{\rm free}$‡ (%) | 18.5 |
| No. of protein atoms | 14459 |
| No. of water molecules | 1586 |
| No. of $Cl^-$ ions | 2 |
| No. of glycerol atoms | 12 |
| Average $B$ factor (Å$^2$) | |
| Overall | 26.30 |
| Protein | 25.60 |
| Water | 32.67 |
| Glycerol | 25.32 |
| $Cl^-$ | 17.58 |
| R.m.s. deviations from ideal geometry | |
| Bond lengths (Å) | 0.016 |
| Bond angles (°) | 1.53 |
| Ramachadran analysis§ | |
| Residues in favoured regions | 1878 [98.5%] |
| Residues in allowed regions | 1907 [100%] |

† Precision-indicating merging $R$ factor $R_{\rm p.i.m.} = \sum_{hkl}[1/(N-1)]^{1/2}\sum_i |I_i(hkl) - \langle I(hkl)\rangle|/\sum_{hkl}\sum_i I_i(hkl)$, where $N$ is the number of observations of reflection $hkl$, $I_i(hkl)$ is the $i$th observation of reflection $hkl$ and $\langle I(hkl)\rangle$ is the average intensity for all observations $i$ of reflection $hkl$. ‡ $R_{\rm work}$ and $R_{\rm free} = \sum_{hkl}\big||F_{\rm obs}| - |F_{\rm calc}|\big|/\sum_{hkl}|F_{\rm obs}| \times 100$ for 95% of the recorded data ($R_{\rm work}$) and 5% of the data excluded from refinement ($R_{\rm free}$). $F_{\rm obs}$ is the observed structure-factor amplitude and $F_{\rm calc}$ is the calculated structure-factor amplitude. § Determined using *MolProbity* (Chen *et al.*, 2010).

cycles of the program *REFMAC* (Murshudov *et al.*, 1997) interspersed with manual checks and rebuilding where required using *Coot* (Emsley & Cowtan, 2004). The quality of the refined model was validated using the programs *PROCHECK* (Laskowski *et al.*, 1993), *SFCHECK* (Vaguine *et al.*, 1999) and finally *MolProbity* (Chen *et al.*, 2010). Refinement statistics are presented in Table 1.

The quaternary structure was analysed using the online *PISA* server (Krissinel & Henrick, 2007) on the European Bioinformatics Institute website. The structure-based sequence alignment was produced with *STRAP* (Gille & Frommel, 2001) and *ALINE* (Bond & Schüttelkopf, 2009). Illustrations of the molecule were produced with *PyMOL* (DeLano Scientific LLC). Secondary-structure elements were determined with *DSSP* (Kabsch & Sander, 1983).

The dynamic domains of porcine SCOT were identified using the *CCP*4 program *DynDom* (Hayward & Berendsen, 1998); the window length was set at 11 residues and the minimum domain size was set at 40 residues. The dynamic domains of YdiF are listed in the *DynDom* nonredundant database (Family ID 735m; Qi *et al.*, 2005) and were recalculated using the *CCP*4 version of the program. Dynamic domains for human SCOT were calculated in the same way using the *CCP*4 version of the program.

**Table 2**
Analysis of subunit contacts in the asymmetric unit.

| Subunit interface | Buried area (Å$^2$) | No. of hydrogen bonds | No. of salt bridges |
|---|---|---|---|
| *A*–*B* | 2316.1 (23%) | 34 | 22 |
| *C*–*D* | 2317.5 (23%) | 33 | 22 |
| *D*–*A* | 150.0 (1%) | 2 | 1 |
| *D*–*B* | 99.1 (1%) | 0 | 0 |

## 3. Results

### 3.1. Overview

The crystal structure determined here belonged to space group $P2_1$, with unit-cell parameters $a$ = 73.72, $b$ = 133.57, $c$ = 102.23 Å, $\beta$ = 104.98°; data-processing statistics are listed in Table 1. The asymmetric unit accommodates four subunits of molecular weight 52 230 kDa, corresponding to a $V_{\rm M}$ of 2.33 Å$^3$ Da$^{-1}$ (Matthews, 1968) and a solvent content of 47.2%. Visual inspection of these four subunits suggested that they formed two dimers and that the dimer–dimer interface has insufficient contacts to maintain a stable tetramer in solution. Analysis of the model using *PISA* (Krissinel & Henrick, 2007) substantiated this interpretation (Table 2) and also confirmed that no alternate tetramer was likely.

The overall fold seen in the structure presented here is the same as that observed in previously reported SCOT structures (Bateman *et al.*, 2002; Coros *et al.*, 2004; Tammam *et al.*, 2007). Subunits *A*, *B* and *D* are in the apo form and superimpose well onto the other known porcine SCOT structures and onto each other. Subunit *C* shows large structural changes and has electron density consistent with a glycerol molecule in its active site.

### 3.2. Glycerol binding in subunit *C*

From the beginning of refinement, clear difference electron density in the shape of a glycerol molecule was observed in the active site of subunit *C*. Towards the end of model building and refinement, a glycerol molecule was modelled into this density. The glycerol-shaped difference density observed in the round of refinement prior to building in the glycerol is shown in Fig. 1. Once included, the glycerol refined well with good geometry and low atomic *B* factors. During the final round of refinement, electron density consistent with a second glycerol molecule was found on the surface of subunit *C*. We interpret this as nonspecific surface binding.

Located in the active site of subunit *C*, the glycerol is stabilized by hydrogen bonds to the catalytic glutamate Glu305 and other active-site residues *via* its three hydroxyl groups. It also makes numerous van der Waals contacts, notably with Phe25 and Tyr76, which partially sandwich one end of the glycerol between them, and with Ile284, which closes in the glycerol at the other end (Fig. 1). The OH1 terminal hydroxyl group of the glycerol forms hydrogen bonds to the ND2 groups of Asn51 (3.3 Å) and Asn52 (2.9 Å), whilst

the OH3 terminal hydroxyl group donates a hydrogen bond to Glu305 OE2 (3.4 Å) and can also accept hydrogen bonds from two water molecules (2.6 and 2.8 Å), which in turn form hydrogen bonds to residues Met384 (2.8 Å) and Ile284 (3.1 Å) *via* their main-chain carbonyl group and main-chain amide group, respectively. The central hydroxyl group, OH2, donates a hydrogen bond to OE2 of the catalytic Glu305 (2.6 Å) and accepts a hydrogen bond from Gln99 NE2 (2.8 Å). The catalytic Glu305 of subunit *C* extends its side chain to point towards the active site and the bound glycerol. In the other subunit of the dimer, subunit *D*, this side chain is in a more bent conformation and forms hydrogen bonds to its main-chain amide and Asn281. These conformations of Glu305 are reminiscent of the different conformations of the glutamyl side chain previously reported in the pig heart SCOT, YdiF and YdiF–CoA complex structures (Rangarajan *et al.*, 2005; Bateman *et al.*, 2002). In the YdiF–CoA complex structure the active-site glutamate adopts one of two extended conformations: conformation I in the thioester intermediate and conformation II in subunits with non-covalently bound CoA. In the apo YdiF structure this residue adopts a bent conformation, conformation III (Rangarajan *et al.*, 2005). The conformation we see here in subunit *C* is similar to conformation II and the conformation in its partner subunit (*D*) without glycerol is comparable to conformation III. All of the residues which interact with the glycerol in subunit *C* do not show significant side-chain conformational changes compared with those of the apo subunits.

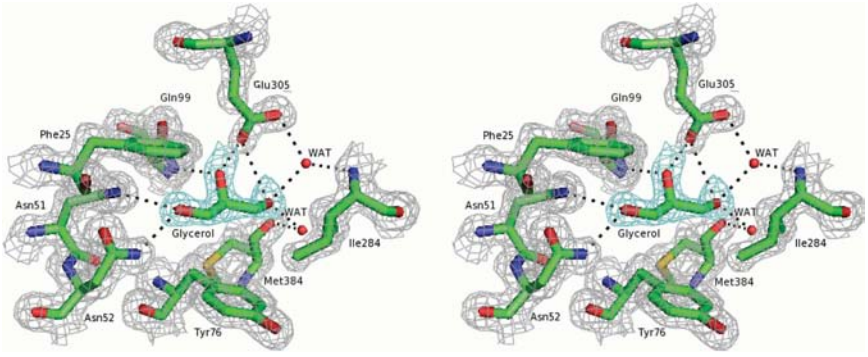


**Figure 1**
Stereo diagram showing the active-site residues that interact with the glycerol molecule in subunit *C* of the SCOT structure presented here. The protein is drawn as sticks and water molecules are drawn as spheres; both are coloured according to atom type (green for carbon, yellow for sulfur, red for oxygen and blue for nitrogen). The difference electron-density map (contoured at 3$\sigma$) around the glycerol molecule calculated prior to building a glycerol molecule into the density is shown in cyan. The $2F_o - F_c$ electron-density map (contoured at 1$\sigma$) around the residues interacting with the glycerol is shown in grey. Possible hydrogen bonds are shown as dotted lines.

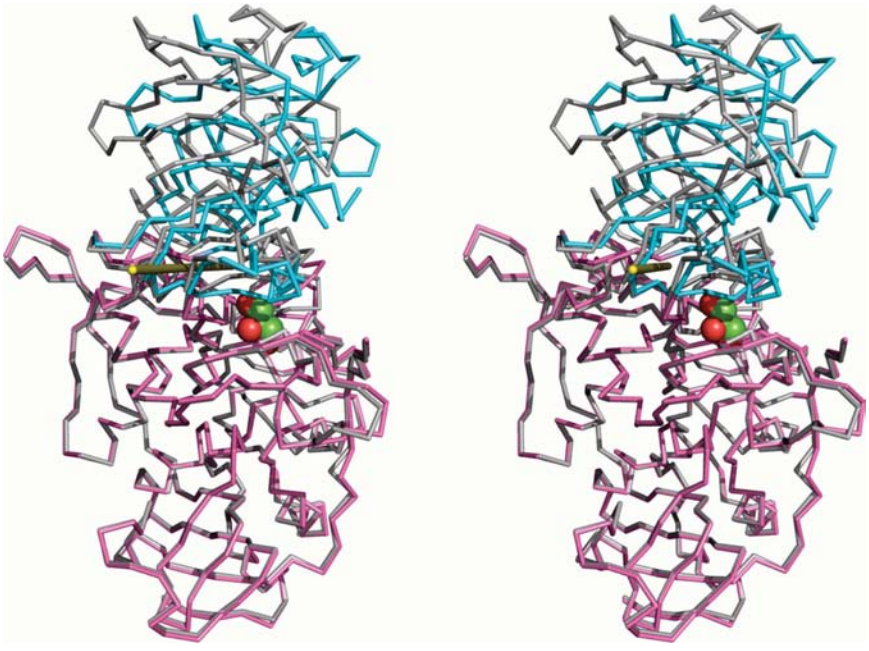

**Figure 2**
Stereoview showing the dynamic domain movement identified in the SCOT structure presented here. Dynamic domain 1 of the glycerol-bound subunit, which is shown in pink for dynamic domain 1 and cyan for dynamic domain 2, is superimposed onto dynamic domain 1 of an apo subunit (subunit *D*) shown in grey. The positional difference between dynamic domain 2 of the glycerol-bound subunit and the apo subunit can be described as a rotation of 13° around a rotation axis shown as a yellow bar in the figure. Both subunits are shown as a backbone trace. The glycerol molecule that we observed bound in the active site of subunit *C* is shown in space-filling representation and coloured by atom type: green for carbon and red for oxygen.

### 3.3. Structural changes in subunit *C*

In our initial examination of the structure, the structural change in the glycerol-bound subunit, although large with an r.m.s. deviation of around 1.6 Å for $C^{\alpha}$ atoms between subunit *C* and subunits *A*, *B* or *D*, was difficult to interpret. When viewed from the perspective of the N- and C-terminal domains it seemed to consist of a number of modules from each which moved independently of their parent domain to close together over the substrate-binding site. However, comparison of the glycerol-bound subunit with the other subunits using the program *DynDom* (Hayward & Berendsen, 1998) revealed two dynamic domains that close by a 13° rotation and a small translation of ∼0.3 Å in the glycerol-bound subunit (Fig. 2). These two dynamic domains, domain 1 and domain 2, have a different residue composition from the N- and C-terminal domains (residues 1–248 and 261–481, respectively). Dynamic domain 1 (pink in Fig. 2) includes the residues of the entire N-terminal domain (1–246) and two clusters of residues from the C-terminal domain (residues 300–358 and 375–394); dynamic domain 2 (cyan in Fig. 2) consists of three clusters of residues from the C-terminal domain (262–299, 359–374 and 395–481).

Two regions at the dynamic domain interface show movements that cannot be described solely by the rigid-body rotation described above and show the following movements additional to the rotation. The first region, comprising of residues 282–292 in dynamic domain 2, moves an additional 0.5–2.5 Å towards the active site and dynamic domain 1. Together with the domain rotation, this leads to many new contacts being made with dynamic domain 1 and the glycerol. Connected residues (261–281 and 293–297) also show smaller movements additional to the dynamic domain rotation; these are either linked to the movement of residues 282–292 or arise in order to avoid steric clashes at the domain interface. The second region consists of residues 373–383 in dynamic domain 1; this was described previously as an 'extended flap' that forms part of the CoA-binding pocket (Rangarajan *et al.*, 2005). It shows an additional movement of up to 2.2 Å compression to avoid steric clashes between the two dynamic domains; this movement is required to accommodate the dynamic domain rotation.

Many new hydrogen bonds are established between the two dynamic domains of subunit *C* after the rigid-body rotation and localized structural changes described above. Mainly formed at the interface of the two domains, these interactions include hydrogen bonds from the hydroxyl group of Ser291 and the side-chain carbonyl of Asn292 to the main-chain carbonyl of Gly312 and the main-chain amide of Tyr314, respectively, from the main-chain carbonyl of Tyr374 to the main-chain amides of both Lys382 and Gly383 and from the main-chain amide of Leu282 to the main-chain carbonyl of Gln303, as well as many water-mediated hydrogen bonds (Table 3).

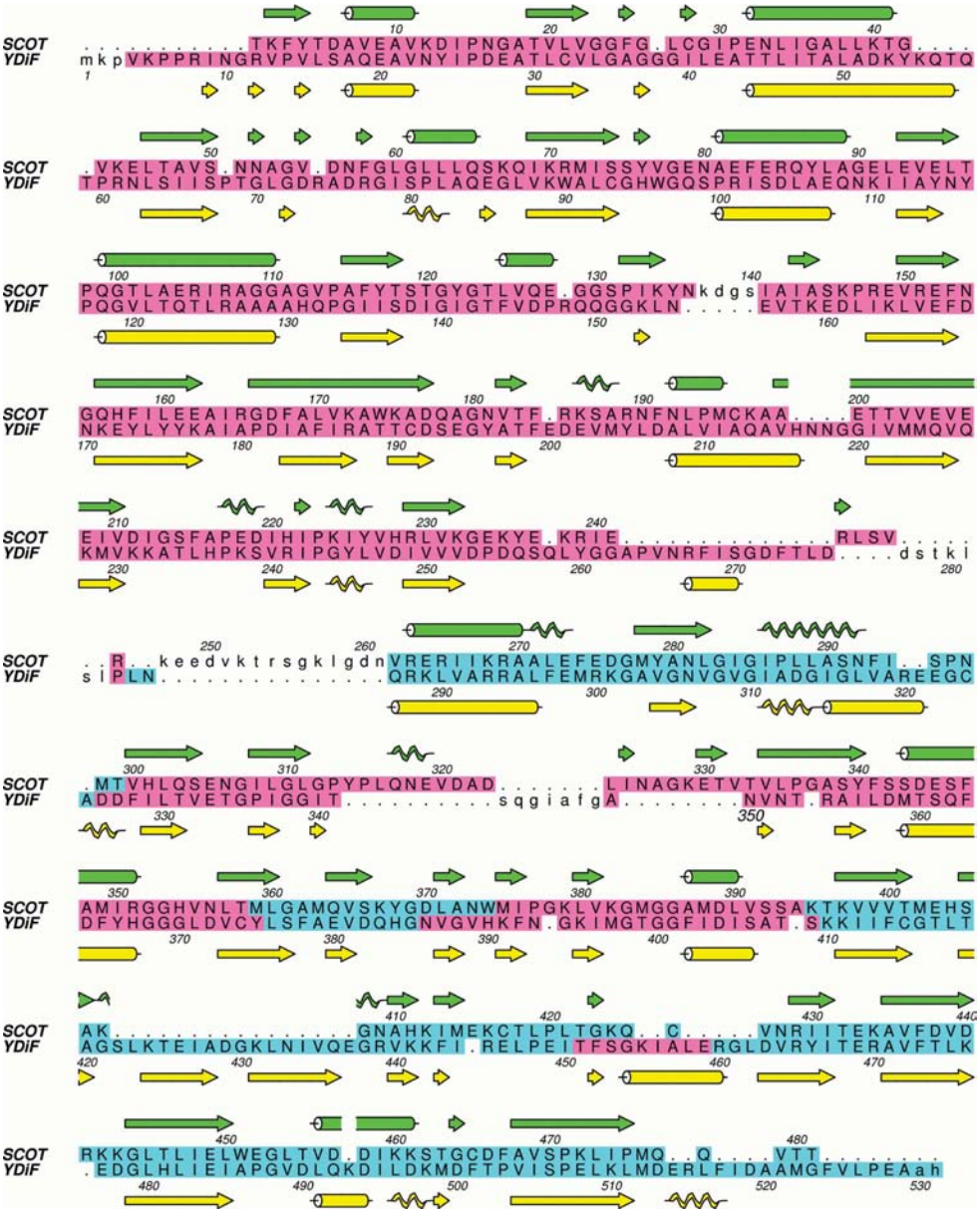


**Figure 3**
Structure-based sequence alignment of pig heart SCOT and *E. coli* YdiF. Secondary structure was determined with *DSSP* (arrows, $\beta$-strands; cylinders, $\alpha$-helices; coils, $3_{10}$-helices) and is shown in green for SCOT and in yellow for YdiF. Residues belonging to dynamic domain 1 have a pink background and those belonging to dynamic domain 2 have a cyan background.

### 3.4. Dynamic domains in other family I CoA trasferases

Recently, the coordinates for the structure of human SCOT, which shares 89% sequence identity with porcine SCOT, have been deposited (PDB code 3dlx). There are four subunits in the asymmetric unit of this structure, none of which contain substrate in the active site. Despite the lack of substrate, structural differences were observed among the four subunits. When we compared the structures of the four subunits with *DynDom* we found that they also have two dynamic domains: subunits *A*, *C* and *D* are closed to various extents (3–6°) compared with subunit *B*, which remains in the open apo form. These dynamic domains are equivalent to those identified in the porcine SCOT structure reported here.

The *E. coli* CoA transferase YdiF has 23% sequence identity to SCOT and shows the highest structural homology to mammalian SCOT of all the structures of type I CoA transferases published to date. Structures of YdiF are available in two forms: the apo protein (PDB code 2ahu)

**Table 3**
List of the new hydrogen bonds formed between the two dynamic domains after domain closure.

The first residue given is from domain 1 and the second is from domain 2.

| | | |
|---|---|---|
| Gly312 O | ··· | Ser291 OG |
| Tyr314 N | ··· | Asn292 OD1 |
| Lys382 N | ··· | Trp374 O |
| Gly383 N | ··· | Trp374 O |
| Gln303 O | ··· | Leu282 N |
| Glycerol | ···$H_2O$··· | Ile284 N |
| Gly361 N | ···$H_2O$··· | Ile284 O |
| Glu305 N | ···$H_2O$··· | Leu282 O |
| Ala327 N | ···$H_2O$··· | Leu282 O |
| Ser304 OG | ···$H_2O$··· | Leu282 O |
| Glu305 OE2 | ···$H_2O$··· | Ile284 N |
| Asn326 ND2 | ···$H_2O$··· | Leu288 O |
| Asn326 ND2 | ···$H_2O$··· | Ser291 OG |
| Leu311 O | ···$H_2O$··· | Ser291 O |

and the glutamyl-CoA thioester intermediate (PDB codes 2ahv and 2ahw). Although no domain movements were identified upon CoA binding in the original structural analysis (Rangarajan *et al.*, 2005), two dynamic domains can be found in the *DynDom* database (Family ID 735m). The CoA-bound intermediates close by between 2.5° and 4° with respect to the apo form. Subunits *A*, *C* and *D* in the apo structure show a marginal closure of 0.5–1° with respect to subunit *B*, reflecting the flexibility of the domains around the hinge point. A structural alignment of YdiF with the SCOT structure reported here shows that the dynamic domains in YdiF are equivalent to those that we have identified in SCOT (Fig. 3).

Although the dynamic domains detected in the porcine SCOT structure presented here are perhaps not compelling on their own, the fact that equivalent dynamic domains can be detected in both the YdiF and human SCOT structures suggests that they are inherent to the fold and are likely to be of functional significance.

### 3.5. Dynamic domains and the dimer interface

Apart from dynamic domain 2 of subunit *C*, dimer *CD* superimposes well with the apo dimer *AB*. Superimposition of the two dimers excluding dynamic domain 2 of both subunits *C* and *B* resulted in a reasonably good r.m.s. deviation of $C^{\alpha}$ atoms of 0.5 Å. A much higher deviation of 1.6 Å is obtained when both the dynamic domains 1 and 2 of subunits *C* and *B* are included. As the overwhelming majority of the residues involved in the intersubunit interaction belong to dynamic domain 1 (the only exceptions are Lys395 and Tyr279) the intersubunit interface of dimer *CD* remains the same as that in the apo dimer *AB*.

When viewed in relation to the dynamic domains, the intersubunit interface is arranged such that the two larger dynamic domains 1 are fixed back to back to form a single unit, with the active sites facing away from each other. The two smaller dynamic domains 2 are free to move on each side (Fig. 4). Dynamic domain 2 of subunit *C* moves from the apo position to close around the active site.

Inspection of the dimer interface lends support to the dynamic domains defined here as opposed to a model in which the N- and C-terminal structural domains move. The dimer interface is stabilized by interactions formed between residues from both the N- and C-terminal structural domains, among which residues 300–358 of the C-terminal domain make a significant contribution. These contacts would be severely disrupted if they were to move to allow the C-terminal domain to close around the active site.

### 3.6. The apo subunits

The three glycerol-free subunits, *A*, *B* and *D*, have apo conformations but their structures are not identical. The structure of subunit *A* is virtually identical to its equivalent in the other dimer, subunit *D*, but differs slightly from its paired partner, subunit *B*. Superimposition of subunit *A* on subunit *D* resulted in an r.m.s. deviation for all $C^{\alpha}$ atoms of 0.45 Å, but a higher r.m.s. deviation of 0.86 Å was observed when it was superimposed on subunit *B*. The main structural differences between subunits *A* and *D* and subunit *B* are in many of the loop residues located on the enzyme surface. Some of the loops adopt different positions to form crystal contacts. One example is a loop consisting of residues 130–142. In subunit *B* this loop adopts a different conformation from its equivalent in subunits *A* and *D*, allowing subunit *B* to make symmetry-related crystal contacts to Leu421 and Thr418 of subunit *C* *via* Asp138 and Ile141. The neighbouring residues of 130–142,

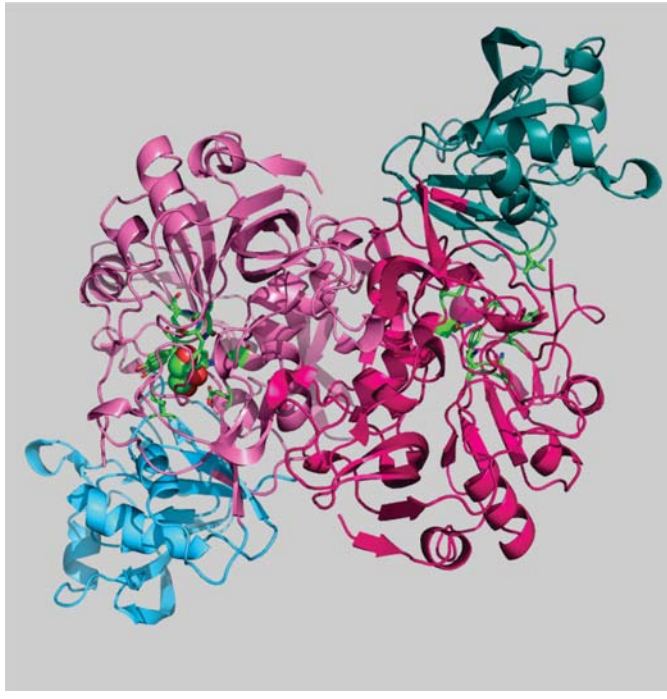

**Figure 4**
Ribbon diagram of the *CD* dimer of SCOT showing the relative orientations of the dynamic domains and the active sites to the dimer interface. The subunit interface in the dimer is composed primarily of residues from dynamic domain 1 (light and dark pink) from each subunit. The smaller dynamic domains (dynamic domain 2; light and dark cyan) play little part in stabilizing the dimer and are free to move independently on binding substrate. The active-site residues are shown as sticks and the glycerol molecule is shown in space-filling representation; both are coloured by atom type (C atoms, green; O atoms, red; N atoms, blue).

residues 80–94 and 376–381, show smaller corresponding changes necessary to accommodate this movement.

Structural differences are also found in some residues in the active site. The catalytic glutamate Glu305 is oriented towards and forms a hydrogen bond to Asn281 in subunits *A* and *D* (conformation III). In subunit *B* it refines with dual occupancy between conformation III and conformation II binding to Glu99. One chloride ion is observed in the active site of subunits *A* and *D* at a position equivalent to that of the chloride ion in the recently reported C28S mutant protein structure (Tammam *et al.*, 2007). The chloride ion has strong electron density in the difference map (peak height 7.2$\sigma$ and occupancy 0.8) and makes hydrogen bonds to Lys329, Asn51 and Asn52 like the chloride ion in the C28S mutant structure. The side chain of Lys329 and its local environment in subunits *A* and *D* adapts in the same way as seen in the C28S mutant structure during chloride ion binding. The Lys329 side chain breaks the hydrogen bonds formed to the carboxyl groups of Glu79 and Glu241 and moves into the active site to approach the chloride ion. The carboxyl group of Glu79, in a concerted movement with several polar or charged side chains in the vicinity, turns away towards the enzyme surface. The polar and charged side chains include that of Lys382, which moves towards Glu79 forming tighter hydrogen bonds, and those of Arg242 and Tyr76, which move away from Glu79. The backbone of residues 77–79 and the following $\alpha$-helix also move accordingly. No chloride ion was found in subunit *B*. The side chain of Lys329 in subunit *B*, like that of Lys329 in subunit *C*, adopts a conformation pointing to the enzyme surface and binding to Glu79 and Glu241. The chloride ions in subunits *A* and *D* would be around 4 Å away from the carboxyl group of Glu305 if its side chain adopted conformation II, repelling the carboxyl group of Glu305 and preventing it from adopting conformation II. The side chain of Glu305 in subunits *A* and *D* can therefore only adopt conformation III.

## 4. Discussion

### 4.1. SCOT–glycerol resembles a CoA-bound intermediate

The closed CoA-bound form of YdiF is closely comparable to our closed glycerol-bound form of SCOT, whereas our apo SCOT structure is opened to a far greater extent than apo YdiF. Overall superimposition of the glycerol-bound SCOT structure onto that of CoA-bound YdiF gives an r.m.s. deviation of 2.6 Å for the 427 aligned $C^{\alpha}$ atoms, compared with 3.4 Å when the apo SCOT structure is used. The similarity between glycerol-bound SCOT and CoA-bound YdiF is particularly striking in two of the CoA-binding components: residues 306–311 and 389–402 of YdiF superimpose upon residues 281–286 and 374–387 of SCOT, respectively, with an average *xyz* displacement of $C^{\alpha}$ atoms of 1.5 Å.

The CoA molecule from the YdiF–CoA structure can be manually docked as a rigid body into the putative CoA-binding site of the glycerol-bound SCOT structure without any significant steric clashes. A few short contacts are observed between CoA and Ile284, but these can be eliminated by small positional changes of the SCOT structure in this region. Furthermore, the CoA molecule docked in the closed glycerol-bound subunit can make many contacts analogous to those in the CoA-bound YdiF structure in both dynamic domains 1 and 2 (Table 4). For example, the main-chain carbonyl of Ile284 and the main-chain amide of Ile286 are positioned to make direct hydrogen bonds to OAP and O5A of CoA, respectively. The guanidinium group of Arg263 is close enough to form an ion pair with the diphosphate group (Fig. 5). When the apo SCOT structure is superimposed onto this SCOT–CoA model, the CoA makes few contacts with SCOT and these are restricted to residues from dynamic domain 1 (with the exception of Met363). The residues in dynamic domain 2 are too far away from the CoA to make contact with it.

**Table 4**
List of interactions between CoA and SCOT in the SCOT–CoA model.

The analogous interactions in the YdiF–CoA complex are shown for comparison. Residues are grouped according to which dynamic domain they belong.

| | YdiF | Interactions | SCOT |
|---|---|---|---|
| Dynamic domain 1 | Val389 | Pantetheine | Asn373 |
| | Phe392 | Adenosine | Ile376 |
| | Met397 | Pantetheine | Lys382 |
| | Thr399 | Pantetheine | Met384 |
| | Phe402 | Pantetheine | Ala387 |
| | Ile405 | Thioester | Leu390 |
| | Glu333 | Thioester | Glu305 |
| Dynamic domain 2 | Val309 | Pantetheine | Ile284 |
| | Gly310 | Pantetheine/diphosphates | Gly285 |
| | Ile311 | Diphosphates | Ile286 |
| | Arg288 | Diphosphate | Arg263 |
| | Ala379 | Adenosine | Met363 |

The region of SCOT equivalent to the third CoA-binding component of YdiF (residues 419–423 and 440–442) does not align well structurally with that of YdiF and is not able to reach the adenine moiety of the CoA as it does in YdiF–CoA. However, this third CoA-binding component of YdiF undergoes structural changes additional to the dynamic domain rotation when it binds to CoA and we would expect the corresponding region in SCOT to change in a similar way in a SCOT–CoA complex.

The strong similarity between the SCOT–glycerol complex and the YdiF glutamyl-CoA thioester intermediate suggests that the SCOT–glycerol structure may resemble the SCOT glutamyl-CoA thioester intermediate. The dynamic domains described here move the molecule from the apo form to what we would expect for a CoA-bound form.

### 4.2. Modelling acetoacetate in the cosubstrate binding site

The glycerol in our structure occupies a site equivalent to that of a chloride ion in the C28S variant SCOT structure (Tammam *et al.*, 2007; PDB code 2nrb). This chloride ion-binding site was proposed to be the cosubstrate-binding site by Tammam and coworkers based on its location, its relative distances from the active-site residues and the fact that anions can inhibit the enzyme activity (Hersh & Jencks, 1967). The glycerol binds in the cosubstrate-binding site and interacts

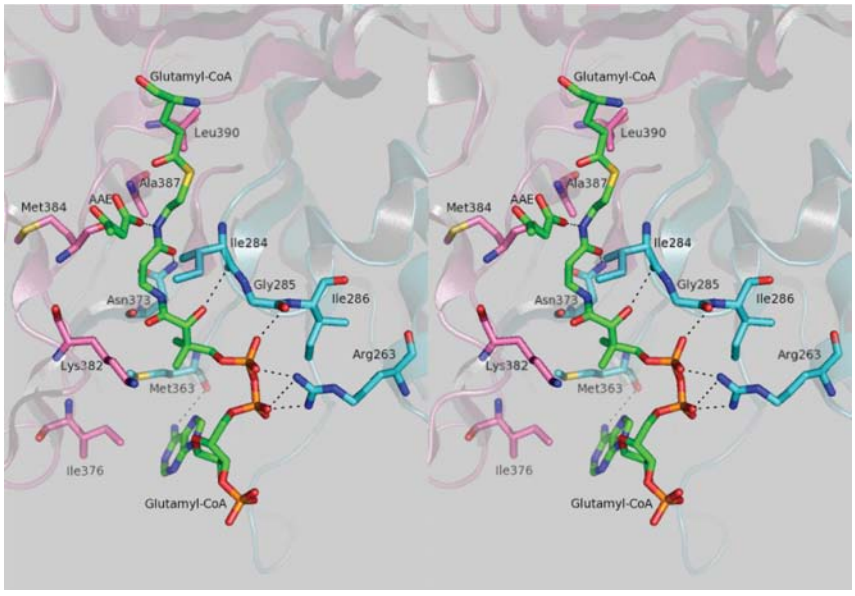


**Figure 5**
Stereo diagram of our proposed model of the porcine SCOT–CoA intermediate showing the predicted interactions between the CoA moiety and SCOT. The cosubstrate, acetoacetate, is shown in the position in which we predict that it would initially bind to the SCOT–CoA intermediate prior to attacking the carbonyl C atom of glutamyl-CoA. Interacting residues, the CoA molecule and acetoacetate (labelled AAE) are shown as sticks and are coloured by atom type: blue for nitrogen, red for oxygen, yellow for sulfur and orange for phosphorus. The C atoms are coloured to emphasize different parts of the structure: pink for dynamic domain 1, cyan for dynamic domain 2 and green for CoA and acetoacetate. Secondary-structure elements follow the same colour scheme and are semi-transparent for clarity; predicted hydrogen bonds are shown as dashes.

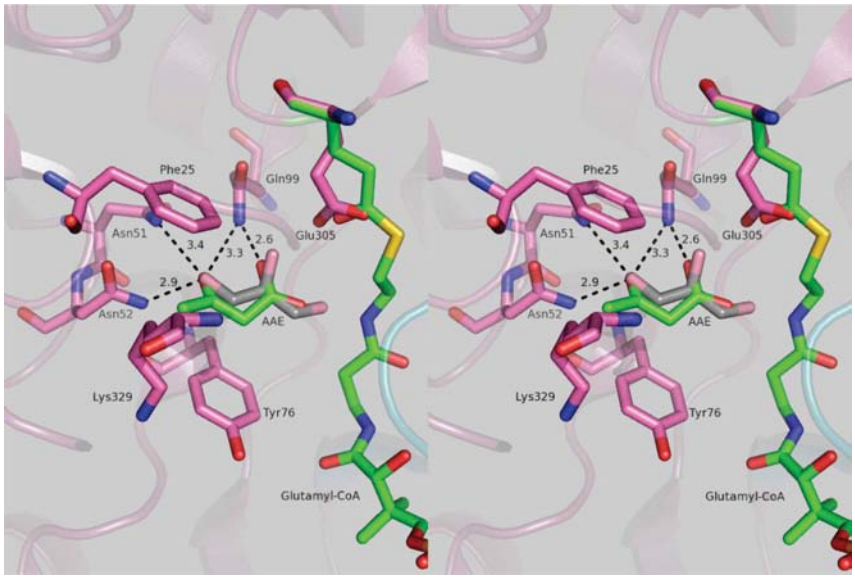


**Figure 6**
Stereoview of predicted acetoacetate binding to porcine SCOT inferred from the binding position of the glycerol in our glycerol-binding subunit. The binding position we observed for the glycerol is shown by a glycerol molecule with C atoms coloured grey and O atoms coloured red; the predicted positions of the acetoacetate and the CoA thioester are shown with C atoms coloured green and O atoms coloured red. The C atoms of the SCOT residues that interact with the glycerol molecule in the SCOT–glycerol complex are shown in pink, with O and N atoms coloured red and blue, respectively. The secondary structure in the region is shown as a transparent cartoon with dynamic domain 1 coloured pink and dynamic domain 2 coloured cyan. The position of the glutamyl thioester was modelled on the YdiF–CoA intermediate with the glutamyl in conformation I (Rangarajan *et al.*, 2005). In this position it would be too far away from the acetoacetate for nucleophilic attack and must move into conformation II (the same conformation as Glu305 in our glycerol-bound subunit) for the reaction to proceed.

with many of the residues with which the cosubstrates would be expected to interact, in particular Glu305 and Gln99. Glycerol molecules are similar to one of the cosubstrates, acetoacetate, in size and to some extent in shape, suggesting that glycerol could mimic acetoacetate. We manually modelled an ideal structure of acetoacetate into the glycerol binding position, matching the carboxyl and carbonyl groups of the acetoacetate to the hydroxyl groups of the glycerol. After some small adjustments to its torsion angles, the acetoacetate fitted into the space occupied by the glycerol without causing any steric clashes. Furthermore, the carboxyl and carbonyl groups are in nearly the same positions as the hydroxyl groups of the glycerol (Fig. 6). The carbonyl group at this position can bind to the ND2 groups of Asn52 and Asn51 and NE2 of Gln99; one of the carboxyl oxygens can also bind to NE2 of Gln99. In our predicted model of SCOT–CoA, the other carboxyl O atom is also within hydrogen-bonding distance of N4P of the pantetheine arm of CoA. The acetoacetate binding orientation modelled here appears to be the optimum orientation for an acetoacetate molecule to bind into the cosubstrate-binding site; the position of Glu305 dictates the direction the carboxyl group should point, the hydrophobic environment created by the long side chain of Lys329 and the aromatic rings of Tyr76 and Phe25 stabilizes the methyl group (C9) and the polar side chains of Asn51, Asn52 and likely Gln99 stabilize the carbonyl group, and the aromatic rings of Tyr76 and Phe25 also sandwich the backbone of the acetoacetate.

A reaction mechanism for family I CoA transferases has been proposed in which the conformation of the active-site glutamate follows the reaction pathway (Rangarajan *et al.*, 2005; Coros *et al.*, 2004). In the enzyme–CoA intermediate of YdiF, Glu333 (the equivalent of Glu305 in SCOT) adopts conformation I and it has been proposed that on binding the cosubstrate it moves to conformation II (with CoA still bound) to enable attack of the carboxyl O atom of the acetoacetate on the carbonyl C atom of the thioester intermediate. Our proposed positioning of acetoacetate based on the glycerol position in the SCOT–glycerol complex supports this scheme: the model of the glutamyl-CoA complex places the carbonyl C atom too far away for attack by the acetoacetate (Glu305 conformation I), but with

Glu305 oriented in an extended conformation similar to conformation II it would be close enough for the reaction to proceed. This suggests that the dynamic domain positions and active-site residues of the SCOT–glycerol complex are in positions similar to those that they would adopt in forming the mixed-anhydride intermediate.

### 4.3. Possible explanations for the dynamic domain movement in SCOT–glycerol

Although domain closure can be found in all of the subunits of the CoA-bound YdiF structures, it is only observed in three subunits of the two dimers in human SCOT and in only one subunit of the two dimers in porcine SCOT. It therefore seems likely that crystal packing has some influence on the domain closure observed in both the structures of porcine and human SCOT. These both lack CoA which is likely to be the natural driver of domain closure.

In the porcine SCOT structure reported here, it is possible that crystal contacts alone are responsible for stabilizing the closed form and an analysis of the crystal contacts lends support to this hypothesis. All of the *C* subunits in the closed conformation line up perpendicular to the dynamic domain rotation axis and parallel to one of the unit-cell axes (*a*) so any shrinkage along this axis could induce the dynamic domain closure. In our earlier 2.4 Å structure (PDB code 1o9l), which belongs to the same space group but has much smaller dynamic domain movements, the *a* unit-cell axis is around 1 Å longer: 74.8 Å compared with 73.7 Å. This shrinkage of the cell could have come about owing to differences in the crystal freezing protocol and could account for the increased domain closure. It is conceivable that only in this crystal-induced closed conformation is the affinity for glycerol high enough to bind a glycerol molecule and that the glycerol molecule bound during crystallization or cryoprotection. An alternative explanation, consistent with the observation that SCOT exhibits half-of-the-sites reactivity (Lloyd & Shoolingin-Jordan, 2001), is that glycerol [which was present at 10%(*v*/*v*) throughout protein purification] was bound to one subunit in each SCOT dimer prior to crystallization and that crystal contacts stabilize the open apo conformation in one of the dimers, releasing the glycerol. In this scenario, we would propose that subunit *B* had lost a glycerol as it shows structural differences from subunits *A* and *D*, which are alike and probably represent the apo subunit in an asymmetric dimer.

## 5. Conclusions

The crystal structure presented here shows clear electron density for a glycerol molecule bound in the active site of one of the subunits in one of the two dimers in the asymmetric unit. This glycerol may bind in an analogous way to one of the natural cosubstrates for the enzyme, acetoacetate. The same subunit also shows large movements of two previously unreported dynamic domains that are distinct from the structural domains usually associated with the enzyme. We have also identified the same dynamic domains in the deposited structures of the human form of the enzyme (PDB code 3dlx) and the distantly related homologue YdiF (PDB codes 2ahu, 2ahv and 2ahw), suggesting that these dynamic domains are intrinsic to this fold and are likely to be of functional importance.

We thank Professor S. P. Wood and Professor J. B. Cooper for critically reading and commenting on this manuscript.

## References

Bateman, K. S., Brownie, E. R., Wolodko, W. T. & Fraser, M. E. (2002). *Biochemistry*, **41**, 14455–14462.
Bond, C. S. & Schüttelkopf, A. W. (2009). *Acta Cryst.* D**65**, 510–512.
Chen, V. B., Arendall, W. B., Headd, J. J., Keedy, D. A., Immormino, R. M., Kapral, G. J., Murray, L. W., Richardson, J. S. & Richardson, D. C. (2010). *Acta Cryst.* D**66**, 12–21.
Collaborative Computational Project, Number 4 (1994). *Acta Cryst.* D**50**, 760–763.
Coros, A. M., Swenson, L., Wolodko, W. T. & Fraser, M. E. (2004). *Acta Cryst.* D**60**, 1717–1725.
Emsley, P. & Cowtan, K. (2004). *Acta Cryst.* D**60**, 2126–2132.
Fukao, T., Kursula, P., Owen, E. P. & Kondo, N. (2007). *Mol. Genet. Metab.* **92**, 216–221.
Fukao, T., Mitchell, G. A., Song, X.-Q., Nakamura, H., Kassovska-Bratinova, S., Orii, K. E., Wraith, J. E., Besley, G., Wanders, R. J., Niezen-Koning, K. E., Berry, G. T., Palmieri, M. & Kondo, N. (2000). *Genomics*, **68**, 144–151.
Gille, C. & Frommel, C. (2001). *Bioinformatics*, **17**, 377–378.
Hayward, S. & Berendsen, H. J. (1998). *Proteins*, **30**, 144–154.
Heider, J. (2001). *FEBS Lett.* **509**, 345–349.
Hersh, L. B. & Jencks, W. P. (1967). *J. Biol. Chem.* **242**, 3468–3480.
Jacob, U., Mack, M., Clausen, T., Huber, R., Buckel, W. & Messerschmidt, A. (1997). *Structure*, **5**, 415–426.
Kabsch, W. & Sander, C. (1983). *Biopolymers*, **22**, 2577–2637.
Koike, R., Amemiya, T., Ota, M. & Kidera, A. (2008). *J. Mol. Biol.* **379**, 397–401.
Korolev, S., Koroleva, O., Petterson, K., Gu, M., Collart, F., Dementieva, I. & Joachimiak, A. (2002). *Acta Cryst.* D**58**, 2116–2121.
Krissinel, E. & Henrick, K. (2007). *J. Mol. Biol.* **372**, 774–797.
Laskowski, R. A., MacArthur, M. W., Moss, D. S. & Thornton, J. M. (1993). *J. Appl. Cryst.* **26**, 283–291.
Lloyd, A. J. & Shoolingin-Jordan, P. M. (2001). *Biochemistry*, **40**, 2455–2467.
Matthews, B. W. (1968). *J. Mol. Biol.* **33**, 491–497.
Murshudov, G. N., Vagin, A. A. & Dodson, E. J. (1997). *Acta Cryst.* D**53**, 240–255.
Murzin, A. G., Brenner, S. E., Hubbard, T. & Chothia, C. (1995). *J. Mol. Biol.* **247**, 536–540.
Navaza, J. (1994). *Acta Cryst.* A**50**, 157–163.
Pickart, C. M. & Jencks, W. P. (1979). *J. Biol. Chem.* **254**, 9120–9129.
Qi, G., Lee, R. & Hayward, S. (2005). *Bioinformatics*, **21**, 2832–2838.
Rangarajan, E. S., Li, Y., Ajamian, E., Iannuzzi, P., Kernaghan, S. D., Fraser, M. E., Cygler, M. & Matte, A. (2005). *J. Biol. Chem.* **280**, 42919–42928.
Rochet, J. C. & Bridger, W. A. (1994). *Protein Sci.* **3**, 975–981.
Solomon, F. & Jencks, W. P. (1969). *J. Biol. Chem.* **244**, 1079–1081.
Song, X., Fukao, T., Watanabe, H., Shintaku, H., Hirayama, K., Kassovska-Bratinova, S., Kondo, N. & Mitchell, G. A. (1998). *Hum. Mutat.* **12**, 83–88.
Tammam, S. D., Rochet, J. & Fraser, M. E. (2007). *Biochemistry*, **46**, 10852–10863.
Vaguine, A. A., Richelle, J. & Wodak, S. J. (1999). *Acta Cryst.* D**55**, 191–205.